Oxid Met (2012) 77:93–106
DOI 10.1007/s11085-011-9275-1

ORIGINAL PAPER

Effect of Oxide Growth Strain in Residual Stresses for the Deflection Test of Single Surface Oxidation of Alloys

Sanjeev Maharjan · Xiancheng Zhang · Zhengdong Wang

Received: 24 May 2011 / Revised: 24 July 2011 / Published online: 13 September 2011

Abstract Residual stresses developed in FeCrAlY and $Ni_{80}Cr_{20}$ alloys have been predicted considering growth strain and creep strain in oxide layer and creep strain in alloy or metal. Such stresses, a net compressive stress developed in oxide scales and a net tensile stress developed in alloy strip, produce deflection of a single surface oxidized specimen during high temperature isothermal oxidation. Stresses generated in these alloys and oxide scales were compared with creep deflections. Introducing oxide growth strain in the oxide scales increase the oxide stress value during the initial oxidation stage, during which creep analysis lacks prediction. Oxide stress reaches maximum value at certain oxidation time in the initial oxidation stage. After that oxidation time relaxation of oxide stress occurs considerably in later oxidation stage.

Keywords Residual stresses · Growth strain · Creep strain · Isothermal oxidation · Relaxation

Introduction

Deflection test has been extensively used to estimate residual stresses during high temperature isothermal oxidation. In this test, a single surface of metal or alloy is oxidized at high temperatures in air forming a protective oxide scales on the exposed surface. Common alloys used to perform such test are $Ni_{80}Cr_{20}$,

S. Maharjan · X. Zhang (✉) · Z. Wang
Key Laboratory of Safety Science of Pressurized System, MOE, College of Mechanical and Power Engineering, East China University of Science and Technology, Meilong Road 130, Shanghai 200237, People's Republic of China
e-mail: xczhang@ecust.edu.cn

S. Maharjan
e-mail: sanjeevworld@yahoo.com

$FeCr_{22}Al_5Y_{0.3}$, $FeCr_{23}Al_5$ and $Ni_{76}Cr_{16}Fe_8$ [1–4]. During oxidation, irrespective of alloy being oxidized or the type of oxide layer formed a net compressive stress in oxide layer and a net tensile stress in metal strip have been reported in several papers [1, 2, 5, 6]. Growth stresses produced are then relieved through bending of oxide/metal composite which can be determined from curvature of the oxide/metal interface. Growths stress of the order of 1.5 GPa on FeCrAlY and 0.5 GPa on NiAl alloys have been reported during high temperature oxidation [7]. Determination of such stresses is important to understand the behavior of mechanical integrity and spallation failure of the oxide scales.

Origin of oxide growth stresses and strain has been manifested in several ways. Pilling and Bedworth described the growth stress based on the molar volume associated with forming an oxide molecule [8]. Rhines and Wolf described addition of oxide lamellae perpendicular to the major metal and oxygen fluxes [9]. Later Clarke [7] described the possible locations of new oxide formed as a result of the inward flux of oxygen and the outward flux of meta ions at the oxide/metal interface, at the top of the oxide layer and at grain boundaries lying parallel to the oxide/metal interface. In these three cases, lateral growth strain would not produce. It would be produced only when new oxide forms along columnar grain boundaries to the interface.

According to Clarke [7], Lateral growth strain is directly proportional to oxide thickness. The equilibrium condition is maintained by proportional constant or growth constant D_{ox}. Lateral growth constant D_{ox} accounts the relative cross sectional areas of the grain boundaries and the grain themselves.

The lateral growth strain was determined as if the oxide layer formed slides over the exposed metallic surface. Actually slipping of the oxide layers is constrained by the underlying metal since deformation of the oxide layer is supposed to be equal to the metal. Constraining oxide deformation produces compressive growth stress in the oxide layer. Compressed oxide layer then induces compressive creep deformation in it. During this process metal also undergoes creep deformation. Thus radius of curvature produced during deformation can be considered due to the growth strain of the oxide layer and creep of both oxide and metal. Previously developed elastic, plastic and creep deflection models have not analyzed such mechanism of deflecting specimen. Elastic condition is applicable when oxidation temperature is low. At higher temperature, stresses predicted by elastic condition are over two orders of magnitude than creep condition for Fecralloy [1]. Plastic condition is used when imposed strain is small. Creep condition is used when stress relaxation occurs due to high temperature oxidation. Though creep condition predicts relaxation of stresses during oxidation it lacks to predict stresses due to growth of oxide layer. Thus a new modeling approach which accounts growth strain and creep strain of oxide layers and that allows instantaneous residual stress determination as well as the sign of these stresses is sought to overcome their limitations.

Therefore, the purpose of this paper is to analyze effect of growth stress in the FeCrAlY alloy and its alumina oxide layers during high temperature isothermal oxidation. First, sensitivity of growth constant D_{ox} on the growth stresses will be observed. Second, location of the neutral axes will be determined from the curvature

of the oxide/metal interface, oxide kinetics and growth constant $D_{ox.}$ Third, planar stress and average stress distribution, based on the position of neutral axes, in the oxide layers and alloy strip will be obtained. Fourth, following above similar methods residual stresses in $Ni_{80}Cr_{20}$ alloy and NiO oxide layers will be analyzed. Finally, stresses developed in these alloys and oxide layers will be compared with creep [10] deformation results to highlight the importance of growth stress.

Deflection and Oxide Kinetics

Fe–22Cr–5Al–0.3Y and $Ni_{80}Cr_{20}$ alloys have been chosen because they form a uniform, adherent scale during short term oxidation [1, 2, 11]. Deflection data of the radius of curvature ρ and rate of change of curvature $\dot{\rho}$ at 1000 °C are available for FeCrAlY alloy [1]. Similarly deflection data of the radius of curvature ρ and rate of change of curvature $\dot{\rho}$ at 900 °C are also available for $Ni_{80}Cr_{20}$ alloy [2]. An oxide scale of thickness h_1 formed on exposed surface of these alloy strips produces deflection δ. When the magnitude of deflection is small compared with the length of the specimen, the deformed strip can be taken as an arc of a circle of radius of curvature ρ which is shown in Fig. 1.

Initial parabolic oxide scale growth h and rate of oxide thickening $\dot{h}$ for the alloy can be expressed in terms of a parabolic rate constant k_p

$$h = k_p t^{\frac{1}{2}} \tag{1}$$

This equation reflects the weight gain measurements of the deflection specimen at the end of the oxidation period. It was assumed that the oxide thickens uniformly over its entire surface. Then mass change can be converted to obtain thickness of the oxide scales. The oxide thickness of scales can be obtained from Eq. 1 and rate of oxide thickness can be obtained differentiating Eq. 1 with oxidation time t. Deflection and oxidation parameter are given in Table 1.

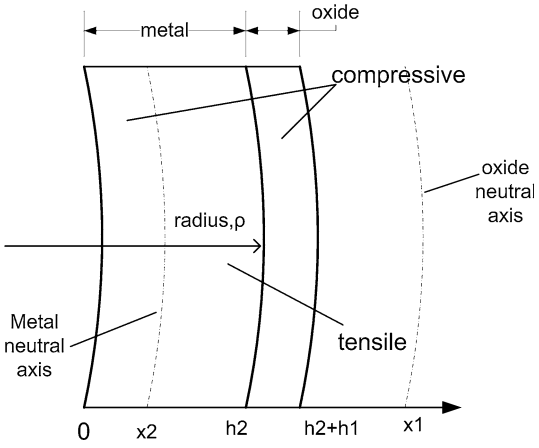

Fig. 1 Coordinate and bending system of oxide/metal composite section for the oxide neutral axis outside the oxide layer

Table 1 Mechanical properties [2, 12], oxide kinetics [1, 2], and creep properties [1, 2] of Fe–Cr–Al–Y alloy oxidized at 1000 °C and $Ni_{80}Cr_{20}$ alloy oxidized at 900 °C

Property	FeCrAlY		$Ni_{80}Cr_{20}$	
	FeCrAlY substrate	Alumina scale	$Ni_{80}Cr_{20}$ substrate	NiO
Parabolic rate constant, k_p ($ms^{-1/2}$)	–	4.864×10^{-9}	–	–
Young's $modulus_{25\ °C,}$ E (GPa)	190	400	–	–
$\frac{dE}{dT}, k$ (GPa/k)	0.09	0.056	–	–
Young's modulus, E (GPa)	102	345 GPa	160	153
Oxide creep index, n_1	–	2.3	–	5.6
Oxide creep constant, A_1 ($Pa^{-n_1}s^{-1}$)	–	4.308×10^{-28}	–	6.145×10^{-53}
Alloy creep index, n_2	5.5	–	4.12	–
Alloy creep constant, A_2 ($Pa^{-n_2}s^{-1}$)	4.947×10^{-43}	–	1.533×10^{-37}	–

Growth and Creep Strain

The growth strain of the oxide is also known as the lateral expansion of the scale that would occur in the absence of constraint by the underlying alloy. Unconstrained oxide growth in the direction normal to the alloy surface does not produce any stress. The growth strain can be expressed in terms of the parabolic rate constant k_p characterizing the oxide thickening with the assumption that both anions and cations flux diffuse along the grain boundaries as

$$\dot{\varepsilon}_G = D_{ox}\dot{h} \tag{2}$$

This equation indicates that in the absence of any stress relaxation the growth strain linearly increase with the oxide thickness [7]. For any particular oxidation time and temperature, it is presumably the same for each specimen but the extent of relaxation in both the oxide and metal depends on the metal/oxide thickness ratio [6].

Actually oxide layer is not free to expand laterally. The substrate alloy constraint produces an in-plane compressive stress in the oxide layer [6]. Simultaneously, the compression causes creep of the oxide. Instantaneous creep rate of such oxide can be expressed as

$$\dot{\varepsilon}_{ox}^{cr} = A_{ox}\sigma_{ox}^{n_{ox}} \tag{3}$$

where σ_{ox} is the planer oxide stress, n_{ox} is the oxide creep index and A_{ox} is oxide creep constant for a given temperature. Therefore the total oxide strain rate during isothermal oxidation is

$$\dot{\varepsilon}_T = \dot{\varepsilon}_G + \dot{\varepsilon}_{ox}^{cr} \tag{4}$$

During oxidation, alloy also deforms leading to stress relaxation in the substrate [11]. Instantaneous creep rate of an alloy can be expressed as

$$\dot{\varepsilon}_{\mathrm{m}}^{cr} = A_{\mathrm{m}}\sigma_{\mathrm{m}}^{n_{\mathrm{m}}} \tag{5}$$

where σ_{m} is the metal planer stress, n_{m} is the metal creep index and A_{m} is metal creep constant for a given temperature. Both creep of the oxide and metal leads to stress relaxation in the scale. These two simultaneous relaxations occur at high temperature and their influence can be determined by the stress values in both phases. During initial oxidation stage scale formed is thin and the tensile stress in the metal is very small. When stresses are generated in the scale, oxide creep is a major relaxation process and metal creep is negligible. As the oxide scale thickens the tensile stress in the alloy increases and leads to alloy deformation [6]. Creep properties of both FeCrAlY alloy and $Ni_{80}Cr_{20}$ alloy and their respective scales are provided in Table 1.

Growth Constant, D_{ox}

Given in Eq. 2, D_{ox} represents slope of a line of the growth strain as a function of oxide scale thickness at particular oxidation temperature. D_{ox} values can be obtained experimentally or estimated theoretically. D_{ox} values obtained from experimental growth strain in the α-Al_2O_3 scale [6, 7] at 1100, 1200 and 1300 °C are presented in Table 2 to show D_{ox} decreases with increasing oxidation temperature for FeCrAlY alloy. It is also important to note that D_{ox} value will remain constant during oxidation exposure irrespective of oxide scale thickness at particular oxidation temperature. In present analysis, D_{ox} value of α-Al_2O_3 scale of FeCrAlY alloy at 1000 °C and D_{ox} value of NiO scale of $Ni_{80}Cr_{20}$ alloy at 900 °C are needed to solve Eqs. 12 and 13 in order to get neutral axes and stresses. But experimental D_{ox} data are unavailable in the literature for these materials at that particular oxidation temperature. As D_{ox} depends on microstructural parameter of oxide scales it can be estimated theoretically at particular oxidation temperature using $D_{ox} = (c/L) \times (\Omega_m/\Omega_{ox})$ [13]. Here $c \leq 1$, L, Ω_m and Ω_{ox} are constant, characteristic macroscopic length, volume of metal per unit of mole and volume of oxide, respectively. For FeCrAlY alloy (Ω_m/Ω_{ox}) is 0.56 and assuming c as 0.6 and L as 50 μm; D_{ox} can be estimated 6840 m^{-1}. Similarly for NiO, (Ω_m/Ω_{ox}) is 0.384 and assuming c as 1 and L as 50 μm; D_{ox} can be estimated 7678 m^{-1}. The aim of this paper is to observe the effect of D_{ox} in stresses rather than calculating exact values of D_{ox}. Thus appropriate D_{ox} values will be varied to see its sensitivity in stresses.

Table 2 Growth constant at various oxidation temperature[a]

Temp. (°C)	1100	1200	1300
Growth constant, D_{ox} (m^{-1})	5128[a]	3636[a]	2400[a]

[a] Approximate D_{ox} values taken from slope of growth strain vs. oxide thickness graph from Ref. [6] for Temp. 1100, 1200 and 1300 °C

Stress Distribution

As already described, the oxide/alloy composite is assumed to deform by pure bending producing curvature of ρ. While bending the planar section of the composite is assumed to remain in plane. Thus strain in any plane is related to its distance $(X - X_n)$ from its neutral axes. Therefore oxide bending strain can be written as

$$\varepsilon_{ox} = \frac{X - X_{ox}}{\rho - h_m + X_{ox}} \qquad \text{for } h_m < X \leq (h_m + h_{ox}) \tag{6}$$

Similarly alloy bending strain as

$$\varepsilon_m = \frac{X - X_m}{\rho - h_m + X_m} \qquad \text{for } 0 < X \leq h_m \tag{7}$$

where $\varepsilon_{ox,m}$ is the planar strain in oxide/alloy plane located at X. For both Eqs. 6 and 7, the denominators give the radius of curvature of the neutral axis for the oxide and alloy, respectively.

Oxide bending strain is produced by the resultant of the growth strain and creep strain of the oxide. Thus oxide bending strain given by Eq. 6 can be related to the total strain of the oxide Eq. 4 to obtain planar oxide stress as

$$\sigma_{ox} = \pm \left\{ abs \left[\frac{(-\dot{\rho})}{A_{ox}} \frac{(X - X_{ox})}{(\rho - h_m + X_{ox})^2} - \frac{D_{ox}}{A_{ox}} \dot{h}_{ox}(t) \right] \right\}^{\frac{1}{n_{ox}}} \tag{8}$$

If the oxide neutral axis X_{ox} lies outside the oxide layer $\sigma_{ox} < 0$ for all $X < X_{ox}$. And if it lies inside the oxide layer $\sigma_{ox} > 0$ for all $X > X_{ox,}$ $\sigma_{ox} = 0$ for $X = X_{ox,}$ and $\sigma_{ox} < 0$ for all $X < X_{ox}$. In other words, when the oxide neutral axis lies outside the oxide layer whole layer of the oxide will be in compression, thus negative sign is used for this condition. When the oxide neutral axis lies inside the oxide layer the oxide region near the outer surface of the oxide will face tensile stress, thus plus sign is used for this condition. Concurrently, remaining oxide region will face compressive stress and negative sign is used.

Alloy bending strain is produced by the creep strain of the alloy. Therefore alloy bending strain given by Eq. 7 can be related to the alloy creep strain given by Eq. 5 to obtain planar alloy stress as

$$\sigma_m = \left\{ abs \left[\frac{(-\dot{\rho})}{A_m} \frac{(X - X_m)}{(\rho - h_m + X_m)^2} \right] \right\}^{\frac{1}{n_m}} \tag{9}$$

If the alloy neutral axis X_m lies within the alloy strip $\sigma_m > 0$ for all $X > X_m$, $\sigma_m = 0$ for $X = X_m$, and $\sigma_m < 0$ for all $X < X_m$.

Equations 8 and 9 give stress distribution of the oxide/alloy composite provided that neutral axes are determined. Equilibrium of forces and moments in the oxide-metal system can be applied at the oxide/metal interface of the composite with width b to obtain neutral axes as

$$b\int_0^{h_m}\sigma_m dx + b\int_{h_m}^{h_m+h_{ox}}\sigma_{ox}dx = 0 \tag{10}$$

And

$$b\int_0^{h_m}\sigma_m x dx + b\int_{h_{ox}}^{h_m+h_{ox}}\sigma_{ox}x dx = 0 \tag{11}$$

This leads to pair of simultaneous equations which when solve numerically provide position of neutral axes. In case of Fe–Cr–Al–Y and $Ni_{80}Cr_{20}$ alloy, the experiment evidence showed that the oxide neutral axis lay outside the oxide layer [1]. At such condition, Eqs. 8 and 9 can be substituted in equilibrium Eqs. 10 and 11 to get simultaneous Eqs. 12 and 13.

$$\begin{aligned}&\frac{n_m}{n_m+1}\left[\frac{(-\dot{\rho})}{A_m}\right]^{\frac{1}{n_m}}\frac{1}{(\rho-h_m+X_m)^{\frac{2}{n_m}}}\left[(h_m-X_m)^{\frac{n_m+1}{n_m}}-(X_m)^{\frac{n_m+1}{n_m}}\right]\\&+\frac{n_{ox}}{n_{ox}+1}\frac{A_{ox}(\rho-h_m+X_{ox})^2}{(-\dot{\rho})}\left\{\left[\frac{(-\dot{\rho})}{A_{ox}(\rho-h_m+X_{ox})^2}(X_{ox}-h_m-h_{ox})-\frac{D_{ox}}{A_{ox}}\dot{h}_{ox}(t)\right]^{\frac{n_{ox}+1}{n_{ox}}}\right.\\&\left.-\left[\frac{(-\dot{\rho})}{A_{ox}(\rho-h_m+X_{ox})^2}(X_{ox}-h_m)-\frac{D_{ox}}{A_{ox}}\dot{h}_{ox}(t)\right]^{\frac{n_{ox}+1}{n_{ox}}}\right\}\end{aligned} \tag{12}$$

And

$$\begin{aligned}&I\left\{\frac{n_m^2}{(n_m+1)(2n_m+1)}\left((X_m)^{\frac{2n_m+1}{n_m}}+(h_m-X_m)^{\frac{2n_m+1}{n_m}}\right)-\frac{n_m h_m(h_m-X_m)^{\frac{n_m+1}{n_m}}}{n_m+1}\right\}\\&+K^{\frac{1}{n_{ox}}}\left\{\frac{n_{ox}}{(n_{ox}+1)}\left[h_m(X_{ox}-h_m-L)^{\frac{n_{ox}+1}{n_{ox}}}-(h_m+h_{ox})(X_{ox}-h_m-h_{ox}-L)^{\frac{n_{ox}+1}{n_{ox}}}\right]\right.\\&\left.+\frac{n_{ox}^2}{(n_{ox}+1)(2n_{ox}+1)}\left[(X_{ox}-h_m-L)^{\frac{2n_{ox}+1}{n_{ox}}}-(X_{ox}-h_m-h_{ox}-L)^{\frac{2n_{ox}+1}{n_{ox}}}\right]\right\}=0\end{aligned} \tag{13}$$

where, $I=\left[\frac{(-\dot{\rho})}{A_m}\right]^{\frac{1}{n_m}}\frac{1}{(\rho-h_m+X_m)^{\frac{2}{n_m}}}$, $K=\frac{(-\dot{\rho})}{A_{ox}}\frac{1}{(\rho-h_m+X_{ox})^2}$ and $L=\frac{D_{ox}\dot{h}_{ox}(t)(\rho-h_m+X_{ox})^2}{(-\dot{\rho})}$.

Simultaneous Eqs. 12 and 13 can be solved for each set of deflection and oxide kinetics parameters to get X_{ox} and X_m. Once these neutral axes are obtained their values can be substituted into Eqs. 8 and 9 to obtain planar stress variation in oxide/alloy composite.

And the average oxide stress where the oxide neutral axis lies outside the oxide layer can be determine as

$$\sigma_{ox} = \frac{n_{ox}}{h_{ox}(n_{ox}+1)} K^{\frac{1}{n_{ox}}} \left\{ [X_{ox} - h_m - h_{ox} - L]^{\frac{n_{ox}+1}{n_{ox}}} - (X_{ox} - h_m - L)^{\frac{n_{ox}+1}{n_{ox}}} \right\} \quad (14)$$

The corresponding average alloy stress is given as

$$\sigma_m = \frac{n_m}{h_m(n_m+1)} \left[\frac{(-\dot{\rho})}{A_m} \frac{1}{(\rho - h_m + X_m)^2} \right]^{\frac{1}{n_m}} \left[(h_m - X_m)^{\frac{n_m+1}{n_m}} - (X_m)^{\frac{n_m+1}{n_m}} \right] \quad (15)$$

Results

Stresses in FeCrAlY Alloy and Alumina Scales

Equations 12 and 13 were solved for the FeCrAlY alloy using the deflections (ρ and $\dot{\rho}$) and oxide kinetics (h_1) data obtained experimentally by Saunders et al. [1]. and the oxidation data presented in Table 1. It was assumed that instantaneous values of these data remain same over oxidation exposure even with the presence of growth strain. Numerical results for locations of the alloy neutral axis and oxide neutral axis are presented in Table 3. From the results, it was concluded that the alloy neutral axis always lies within alloy strip where as the oxide neutral axis always lies outside the oxide layer.

The location of the alloy neutral axis moves toward oxide/metal interface during oxidation exposure as shown in Fig. 2. As an example for D_{ox} 10,000 m^{-1}, the alloy neutral axis lies at 3.403 $\times$ 10^{-5} m when t is 0.5 h and it moves toward oxide/metal interface i.e. 7.228 $\times$ 10^{-5} m when t is 6.5 h. But at particular oxidation exposure time the location of the alloy neutral axis moves toward unoxidized surface of the alloy with increase of D_{ox} values. For example, at $t = 0.5$ h, alloy neutral axis lies at 6.05 $\times$ 10^{-5} m for Saunders model (creep model or $D_{ox} = 0$ m^{-1}) where as it lies at 3.403 $\times$ 10^{-5} m for D_{ox} 10,000 m^{-1}. At $t = 6.5$ h similar behavior can be seen in Fig. 2. It also means that location of the alloy neutral axis is always smaller than creep model. It can be note in Fig. 2 that the width between $D_{ox} = 10{,}000$ m^{-1} and Saunders ($D_{ox} = 0$ m^{-1}) decrease with increase of oxidation time.

Table 3 Neutral axes for FeCrAlY alloy oxidized at 1000 °C

t, hours	$D_{ox} = 5000$ m^{-1}		$D_{ox} = 7500$ m^{-1}		$D_{ox} = 10{,}000$ m^{-1}	
	X_{ox}, m	X_m, m	X_{ox}, m	X_m, m	X_{ox}, m	X_m, m
0.5	1.485×10^{-3}	4.783×10^{-5}	2.021×10^{-3}	4.077×10^{-5}	2.579×10^{-3}	3.403×10^{-5}
1.0	9.52×10^{-4}	4.72×10^{-5}	1.245×10^{-3}	4.237×10^{-5}	1.548×10^{-3}	3.741×10^{-5}
1.5	7.132×10^{-4}	5.31×10^{-5}	9.274×10^{-4}	4.916×10^{-5}	1.144×10^{-3}	4.532×10^{-5}
2.0	5.88×10^{-4}	6.08×10^{-5}	7.626×10^{-4}	9.538×10^{-5}	9.364×10^{-4}	5.477×10^{-5}
3.0	4.924×10^{-4}	6.66×10^{-5}	6.286×10^{-4}	6.459×10^{-5}	7.67×10^{-4}	6.18×10^{-5}
4.0	4.427×10^{-4}	7.195×10^{-5}	5.59×10^{-4}	7.039×10^{-5}	6.77×10^{-4}	6.803×10^{-5}
5.0	4.1×10^{-4}	7.59×10^{-5}	5.151×10^{-4}	7.261×10^{-5}	6.198×10^{-4}	6.976×10^{-5}
6.5	3.83×10^{-5}	7.72×10^{-5}	4.742×10^{-4}	7.442×10^{-5}	5.65×10^{-4}	7.228×10^{-5}

It is obvious from the Fig. 2 that compressive stress exists for the portion between unoxidized surface (i.e. x = 0 m) of the alloy and the alloy neutral axis where as tensile stress exists between the alloy neutral axis and the oxide/alloy interface (i.e. $x = h_2$). It is interesting to note that tensile metal stresses obtained in present analysis are greater than creep analysis where as compressive metal stresses are smaller than creep analysis. For each curves, the stress distribution calculated using Eq. 9 shows that tensile peak stress and compressive peak stress were around ±2.5 MPa and −2 MPa, respectively. But the average stress calculated from Eq. 15 will always be tensile. The average tensile stress increases with increase of D_{ox} values. In present analysis as well as in creep analysis the average tensile stress value decreases during oxidation exposure due to creep relaxation of alloy.

In the oxide layers, the planar stress is compressive everywhere. Planar stress at $t = 0.5$ h and $t = 6.5$ h are shown in Figs. 3 and 4, respectively. During initial oxidation i.e. $t = 0.5$ h, planar stress is same everywhere for the thin oxide scale i.e. 0.207 μm. As the oxide scale thickens i.e. 0.744 μm during oxidation exposure i.e. $t = 6.5$ h slight variation of planar stress can be noticed in Fig. 4. Another things to note from the Figs. 3 and 4 are planar oxide increase with increase of D_{ox} and is greater than creep model's planar stress. The average oxide stress is shown in Fig. 5. The maximum average compressive oxide stress occurred at $t_{max} = 0.5$ h. It can be seen that maximum compressive stress value increased due to the presence of D_{ox}. Such results have been reported in several literatures [6, 14]. After t_{max} oxidation time considerable relaxation of oxide stress occurred due to creep relaxation of both oxide scales and alloy.

Stresses in $Ni_{80}Cr_{20}$ Alloy and NiO Scales

Similarly neutral axes and residual stresses were obtained for $Ni_{80}Cr_{20}$ alloy. For this deflections and oxidation data obtained experimentally by Huntz et al. [2] were used. Numerical solutions of neutral axes used to obtain residual stresses are presented in Table 4. From the results, it was observed that conclusions drawn for the location of the alloy neutral axes, tensile and compressive alloy stress to

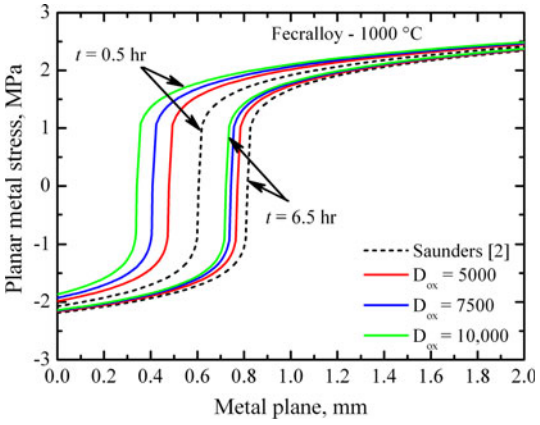

Fig. 2 Stress distribution across 0.2 mm Fecralloy substrate at the respective oxidation time and D_{ox} value

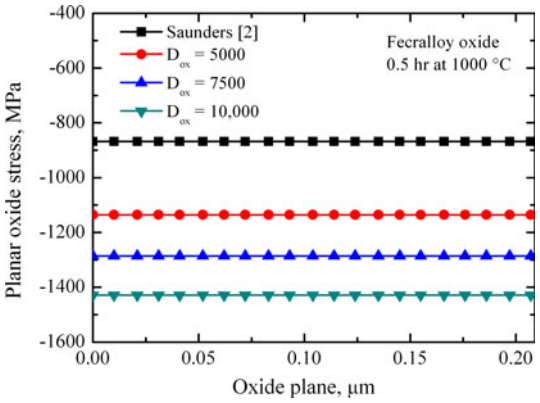

Fig. 3 Stress distribution across 0.207 μm oxide layer after 0.5 h exposure for Fecralloy. The respective case corresponds to the alloy stress distribution shown in Fig. 2

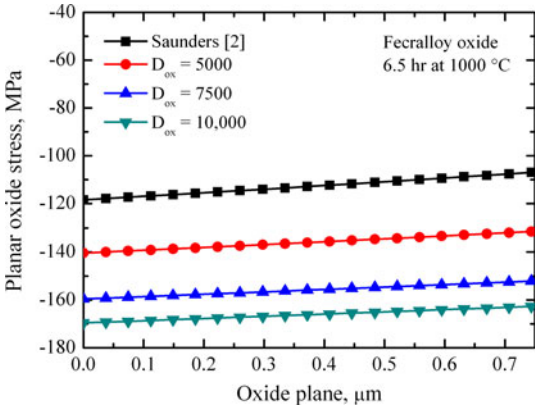

Fig. 4 Stress distribution across 0.744 μm oxide layer after 6.5 h exposure for Fecralloy. The respective case corresponds to the alloy stress distribution shown in Fig. 2

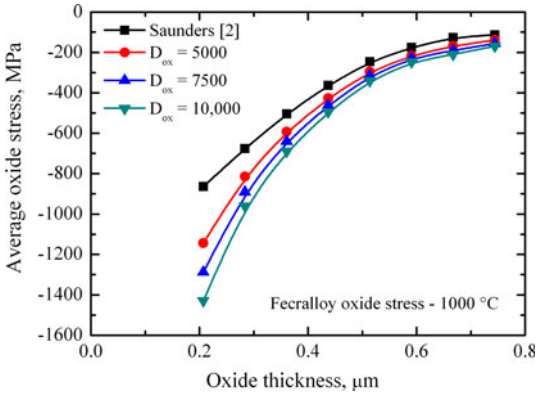

Fig. 5 Average oxide variation with oxidation exposure and corresponding oxide thickness for Fecralloy

FeCrAlY alloy are also applicable to $Ni_{80}Cr_{20}$ alloy. In contrast to the FeCrAlY alloy, location of the alloy neutral axis moves toward unoxidized surface of $Ni_{80}Cr_{20}$ alloy during oxidation exposure. Planar metal stress distributions at 0.1 and 1 h oxidation are given in Figs. 6 and 7, respectively. Planar metal stresses were

Table 4 Neutral axes for $Ni_{80}Cr_{20}$ alloy oxidized at 900 °C

t, hours	$D_{ox} = 5000\ m^{-1}$		$D_{ox} = 10{,}000\ m^{-1}$		$D_{ox} = 20{,}000\ m^{-1}$	
	X_{ox}, m	X_m, m	X_{ox}, m	X_m, m	X_{ox}, m	X_m, m
0.05	0.032	3.786×10^{-5}	0.0442	3.751×10^{-5}	0.0783	3.640×10^{-5}
0.01	0.0334	3.115×10^{-5}	0.0445	3.052×10^{-5}	0.0751	2.899×10^{-5}
0.15	0.0306	2.70×10^{-5}	0.0401	2.63×10^{-5}	0.0742	2.417×10^{-5}
0.2	0.0301	2.364×10^{-5}	0.0392	2.287×10^{-5}	0.0725	2.048×10^{-5}
0.25	0.0299	2.09×10^{-5}	0.0394	2×10^{-5}	0.0709	1.766×10^{-5}
0.3	0.0291	1.88×10^{-5}	0.0388	1.778×10^{-5}	0.0689	1.543×10^{-5}
0.35	0.0281	1.706×10^{-5}	0.0385	1.584×10^{-5}	0.0689	1.339×10^{-5}
0.4	0.0272	1.56×10^{-5}	0.0381	1.418×10^{-5}	0.0681	1.175×10^{-5}
0.45	0.0264	1.427×10^{-5}	0.0381	1.267×10^{-5}	0.0677	1.016×10^{-5}
0.5	0.0258	1.316×10^{-5}	0.0374	1.143×10^{-5}	0.0673	8.9×10^{-6}
0.55	0.0255	1.196×10^{-5}	0.0373	1.022×10^{-6}	0.0658	7.72×10^{-6}
0.6	0.0250	1.108×10^{-5}	0.0364	9.274×10^{-6}	0.0659	6.65×10^{-6}
0.65	0.0244	1.029×10^{-5}	0.0361	8.327×10^{-6}	0.0639	5.84×10^{-6}
0.7	0.0231	9.723×10^{-6}	0.0353	7.52×10^{-6}	0.0627	4.952×10^{-6}
0.75	0.0230	8.88×10^{-6}	0.0335	7.012×10^{-6}	0.0620	4.108×10^{-6}
0.8	0.0231	8.11×10^{-6}	0.0329	6.326×10^{-6}	0.0613	3.367×10^{-6}
0.85	0.0229	7.42×10^{-6}	0.0321	5.729×10^{-6}	0.0592	2.769×10^{-6}
0.9	0.0218	7.11×10^{-6}	0.0314	5.159×10^{-6}	0.0581	2.195×10^{-6}
0.95	0.0214	6.586×10^{-6}	0.0309	4.598×10^{-6}	0.0578	1.481×10^{-6}
1.0	0.0211	6.03×10^{-6}	0.0301	4.138×10^{-6}	0.0577	7.36×10^{-7}

compared with creep model presented by Huntz et al. [2] (creep model or $D_{ox} = 0\ m^{-1}$) with a slight modification for location of metal neutral axis. They assumed location of the metal neutral axis a constant value of 5×10^{-5} m during entire oxidation. But in present comparison the location of metal neutral axis was assumed to constrain between unoxidized surface of metal and metal/oxide interface. For 0.1 h oxidation exposure, peak compressive and tensile stresses were obtained similar in both analysis i.e. about -17 MPa and ± 21 MPa which is shown in Fig. 6. And after1 h oxidation exposure, peak tensile stresses were obtained still similar both being about ± 15 MPa. But peak compressive stress was found smaller than creep results i.e. -5 MPa when D_{ox} is $10{,}000\ m^{-1}$. It can be seen that increasing D_{ox} value decreases peak compressive stress in the alloy strip.

Planar oxide stresses are presented in Figs. 8 and 9 for 0.1 h and 1 h oxidation exposure, respectively. Planar oxide stresses are compressive for entire NiO scales. Planar oxide stresses increase with increase of D_{ox} values. Planar oxide stresses are found greater than creep model results. Planar oxide stresses remain constant in all oxide scales during entire oxidation exposure.

Average oxide stresses are presented in Fig. 10. The average oxide stress increase during initial oxidation stage. It attains maximum compressive stress at $t_{max} = 0.1$ h. After that oxidation time average oxide stress decreases curvilinearly

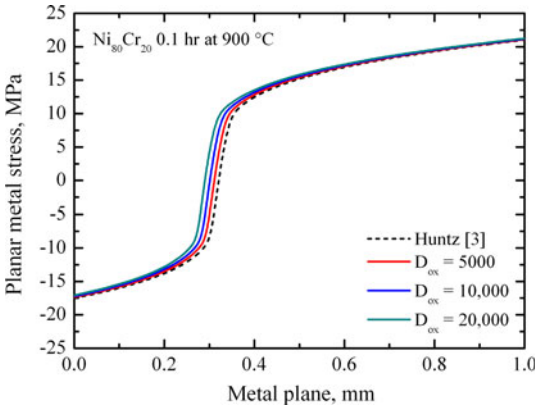

Fig. 6 Stress distribution across 0.1 mm thick $Ni_{80}Cr_{20}$ alloy at oxidation time $t = 0.1$ h

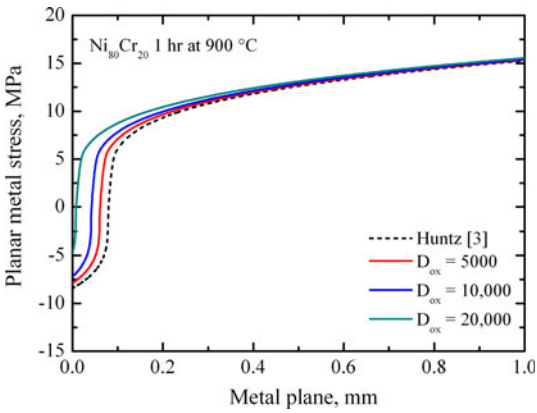

Fig. 7 Stress distribution across 0.1 mm thick $Ni_{80}Cr_{20}$ alloy at oxidation time $t = 1$ h

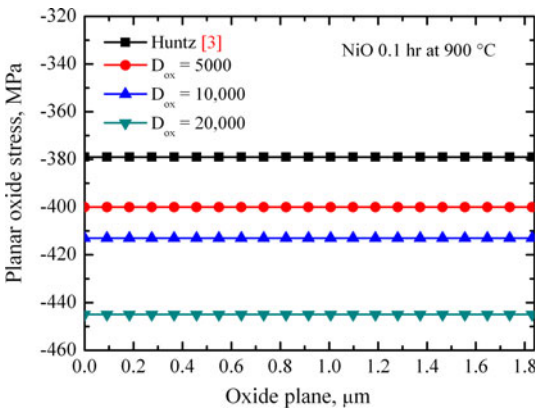

Fig. 8 Stress distribution across 1.83 µm oxide layer after 0.1 h exposure for $Ni_{80}Cr_{20}$ alloy. The respective case corresponds to the metal stress shown in Fig. 6

till the end of oxidation exposure time. Average oxide stresses obtained are greater than creep model. Also, Maximum compressive average oxide stress value increases with increase of D_{ox}.

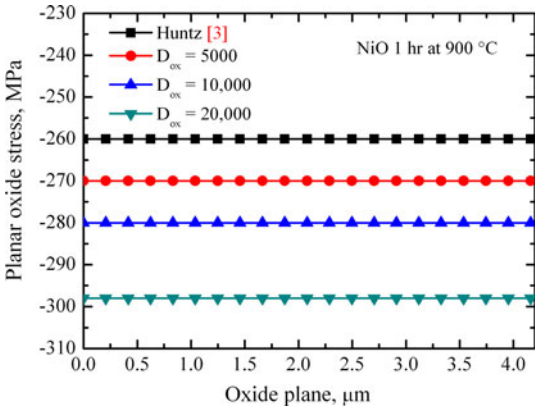

Fig. 9 Stress distribution across 4.16 μm oxide layer after 1 h exposure for $Ni_{80}Cr_{20}$ alloy. The respective case corresponds to the metal stress shown in Fig. 7

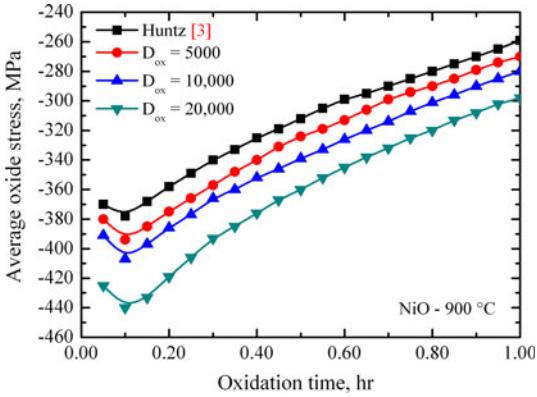

Fig. 10 Average oxide stress variation with oxide thickness for $Ni_{80}Cr_{20}$ alloy

Conclusions

A re-analysis of stress distribution within oxide/alloy composite when a specimen deflects during isothermal oxidation considering growth strain of oxide and creep strain of both oxide and alloy has been provided in this paper for the Fecralloy and $Ni_{80}Cr_{20}$ alloy. For both alloys, oxide neutral axis always lies outside the oxide layer where as alloy neutral axis always lies inside alloy strip with the presence of growth stress. In both alloys, oxide neutral axis moves towards outer surface of oxide layer during oxidation. In Fecralloy, metal neutral axis moves towards oxide/alloy interface, but in $Ni_{80}Cr_{20}$ alloy it moves toward unoxidized surface of alloy, to maintain equilibrium of a net compressive stress produced in the oxide layer and a net tensile stress produced in the alloy.

A comparison of present analysis was made with creep analysis. Present analysis illustrated increment of oxide stress by introducing growth strain during initial oxidation stage for both alloys which creep analysis could not predict. But alloy stress showed two different results. It was decreased in the Fecralloy and increased in the $Ni_{80}Cr_{20}$ alloy during oxidation exposure. Thus it highlights the importance of

growth stress and creep deformation of the composite to predict realistic stresses for the deflection test specimen during high temperature oxidation.

References

1. S. R. J. Saunders, H. E. Evans, M. Li, D. D. Gohil, and S. Osgerby, *Oxidation of Metals* **48**, 189 (1997).
2. A. M. Huntz, G. C. Amiri, H. E. Evans, and G. Cailletaud, *Oxidation of Metals* **57**, 499 (2002).
3. J. G. Zhao and A. M. Huntz, *Journal of Material Science* **19**, 3166 (1984).
4. M. Li, T. Li, W. Gao, and Z. Liu, *Oxidation of Metals* **51**, 333 (1999).
5. H. E. Evans, *International Materials Reviews* **40**, 1 (1995).
6. V. K. Tolpygo, J. R. Dryden, and D. R. Clarke, *Acta Materialia* **46**, 927 (1998).
7. D. R. Clarke, *Acta Materialia* **51**, 1393 (2003).
8. N. B. Pilling and R. E. Bedworth, *Journal Institute of Metals* **29**, 529 (1923).
9. F. N. Rhines and J. S. Wolf, *Metallurgical and Materials* **1**, 1701 (1970).
10. H. E. Evans, *Materials Science and Engineering* **A203**, 117 (1995).
11. V. K. Tolpygo and D. R. Clarke, *Oxidation of Metals* **49**, 187 (1998).
12. S. J. Bull, *Oxidation of Metals* **49**, 1 (1998).
13. B. Panicaud, J. L. Grosseau-Poussard, and J. F. Dinhut, *Computational Materials Science* **42**, 286 (2008).
14. B. Panicaud, J. L. Grosseau-Poussard, and J. F. Dinhut, *Applied Surface Science* **252**, 5700 (2006).